Electronic Supplementary Information

Enhancement of Oxygen Surface Exchange on Epitaxial $La_{0.6}Sr_{0.4}Co_{0.2}Fe_{0.8}O_{3-\delta}$ Thin Films using Advanced Heterostructured Oxide Interface Engineering

Dongkyu Lee,[1,2,5] Yueh-Lin Lee,[1,2] Xiao Renshaw Wang,[1,2] Dane Morgan,[4] and Yang Shao-Horn[1,2,3,*]

[1]Electrochemical Energy Laboratory, [2]Department of Mechanical Engineering, and [3]Department of Materials Science and Engineering, Massachusetts Institute of Technology, 77 Massachusetts Avenue, Cambridge, Massachusetts 02139, United States[4]

[5]*Department of Materials Science and Engineering, University of Wisconsin–Madison, 1509 University Avenue, Madison, Wisconsin 53706, United States*

[5]*Materials Science and Technology Division, Oak Ridge National Laboratory, Oak Ridge, Tennessee 37831, United States*

Index **Page**

Experimental details

Target Synthesis. Both $La_{0.6}Sr_{0.4}Co_{0.2}Fe_{0.8}O_{3-\delta}$ ($LSCF_{113}$) and $LaSrCoO_{4\pm\delta}$ (LSC_{214}) were prepared by the Pechini methods. $La(NO_3)_3 \bullet 6H_2O$, $Co(NO_3)_3 \bullet 6H_2O$, $Fe(NO_3)_3 \bullet 9H_2O$, $Sr(NO_3)_2$, and separately $La(NO_3)_3 \bullet 6H_2O$, $Co(NO_3)_3 \bullet 6H_2O$, $Sr(NO_3)_2$ were dissolved in de-ionized water with ethylene glycol, and citric acid (Sigma-Aldrich, USA) mixture to synthesize $LSCF_{113}$ and LSC_{214} respectively. After esterification at 100 ºC, the resin was charred at 400 ºC and finally calcined at 1000 ^{o}C in air for 12 hours. The $La_{0.8}Sr_{0.2}CoO_{3-\delta}$ (LSC_{113}) and $Gd_{0.2}Ce_{0.8}O_2$ (GDC) were also prepared by the Pechini methods[1]. $La(NO_3)_3 \bullet 6H_2O$, $Sr(NO_3)_2$, $Mn(NO_3)_2 \bullet 6H_2O$, and separately $Gd(NO_3)_3$ and $Ce(NO_3)_3$ were dissolved in de-ionized water with ethylene glycol, and citric acid (Sigma-Aldrich, USA) mixture to synthesize LSC_{113} and GDC respectively. After esterification at 100 ºC, the resin was charred at 400 ºC and finally calcined at 1000 ^{o}C in air for 12 hours. Pulsed laser deposition (PLD) target pellets with 25 mm diameter were subsequently fabricated by uniaxial pressing at 50 MPa. The $LSCF_{113}$, LSC_{113}, LSC_{214}, and GDC pellets were fully sintered at 1,300 ºC in air for 6 hours, 1,200 ºC in air for 10 hours, 1,350 ºC in air for 12 hours, and 1,100 ºC in air for 14 hours, respectively.

Sample preparation. Single crystal 9.5 mol% Y_2O_3-stabilized ZrO_2 (YSZ) wafers with (001) orientation and dimensions of 10 × 5 × 0.5 mm (MTI corporation, USA), were used as substrate. Prior to LSC_{214}, $LSCF_{113}$, LSC_{113}, and GDC deposition, platinum ink (Pt) (#6082, BASF, USA) counter electrodes were painted on one side of the YSZ and dried at 900 ºC in air for 1 hour. PLD was performed using a KrF excimer laser at λ = 248 nm, 10 Hz pulse rate and 45 mJ pulse energy under $p(O_2)$ of 50mTorr with 500 pulses of GDC (~5 nm) at 550 °C, followed by 15,000

pulses of $LSCF_{113}$ (~63 nm) at 650 ºC. Immediately after completing the $LSCF_{113}$ base film deposition, LSC_{214} and LSC_{113} films were subsequently deposited. After completing the final deposition, the sample was cooled to room temperature in the PLD chamber for ~1 hour under an oxygen partial pressure of 50 mTorr. The film thicknesses were determined by atomic force microscopy (AFM). The utilization of reflection high-energy electron diffraction (RHEED) enabled diagnostic *in-situ* monitoring of the $LSCF_{113}$ film growth.

Relaxed lattice parameter determination by HRXRD. The Relaxed lattice parameter $\hat{a}$ and $\hat{c}$ are derived from the following equation (where $\hat{a}$ and $\hat{c}$ are the relaxed lattice parameters for the film in an unstrained state),[2-4] $\frac{(c-\hat{c})}{\hat{c}} = \frac{-2\nu}{1-\nu}\frac{(a-\hat{a})}{\hat{a}}$, assuming $\hat{a} = \hat{c}$, and $\nu = 0.25$.[2] The in-plane strain is given by: $\varepsilon_{aa} = \frac{(a-\hat{a})}{\hat{a}}$ and the out of plane strain by: $\varepsilon_{cc} = \frac{(c-\hat{c})}{\hat{c}}$

Microelectrodes Fabrication. *In situ* electrochemical impedance spectroscopy (EIS) measurements were conducted to probe ORR activity on geometrically well-defined $LSCF_{113}$ with single-layer and double-layer decoration microelectrodes fabricated by photolithography and acid etching, where sintered porous Pt sintered onto the backside of the YSZ substrate served as the counter electrode. OCG positive photoresist (Arch Chemical Co., USA) was applied on the surface of the samples and patterned using a mask aligner (Karl Süss, Germany, λ = 365 nm). The photoresist was developed using Developer 934 1:1 (Arch Chemical Co., USA) and the thin films were etched in hydrochloric acid (HCl) to remove the $LSCF_{113}$ with single-layer and double layer decoration films excess and create the circular microelectrodes (diameters ~50 μm, ~100 μm, ~150 μm, and ~200 μm, exact diameter determined by optical microscopy). Before

electrochemical testing, microelectrode geometry and morphology was examined by optical microscopy (Carl Zeiss, Germany) and atomic force microscopy (AFM) (Veeco, USA).

Electrochemical Characterization. Fig. S4(b) and S4(c) detail the equivalent circuit and corresponding Nyquist plot for this experimental system. *ZView* software (Scribner Associates, USA) was used to construct the equivalent circuit and perform complex least squares fitting. The EIS data were fitted using a standard resistor (R_1) for *HF* and resistors (R_2) in parallel with a constant phase elements (CPE_2) for *MF* and *LF* (R_1-(R_2/CPE_2)-(R_{ORR}/CPE_{ORR})). Based on the $p(O_2)$ dependence of the three features, physical or chemical process with regard to each frequency range can be determined.[5-8] The *HF* feature was found unchanged with $p(O_2)$, and its magnitude and activation energy (~1.15 eV) were comparable to those of oxygen ion conduction in YSZ reported previously[9]. The *MF* feature, which was found to have a $p(O_2)$ independent feature, was attributed to interfacial transport of oxygen ions between the $LSCF_{113}$ film and the GDC layer. In addition, the magnitude of its capacitance was relatively small (~10^{-6} F) compared to the *LF* feature (~10^{-3} F). The *LF* feature was found to have a strong $p(O_2)$ dependence. The resistance of the *LF* feature drastically increases as oxygen partial pressure decreases. In the case of thin film samples, the magnitude of capacitance is due to the oxygen content change in the films. Therefore, the electrode oxygen surface reaction corresponds with the *LF* feature. We obtained values for R_{ORR} and knowing the area of the microelectrode ($A_{electrode} = 0.25\ \pi\ d_{electrode}^2$). Then, we can determine the ORR area specific resistance ($ASR_{ORR} = R_{ORR} \cdot A_{electrode}$). The electrical surface exchange coefficient (k^q), which is comparable to k^*,[10] was determined using the expression,[11, 12]

$$k^q = RT / 4F^2 R_{ORR} A_{electrode} c_o \quad (1)$$

where R is the universal gas constant (8.314 J mol^{-1} K^{-1}), T is the absolute temperature, F is the Faraday's constant (96,500 C mol^{-1}), and c_o is the lattice oxygen concentration in $LSCF_{113}$ where

$$c_o = (3-\delta)/V_m, \quad (2)$$

V_m is the molar volume of $LSCF_{113}$ at room temperature. In this study, c_o was calculated with δ extracted from previous reported values[13].

The surface coverage may change the c_o value of the system. For estimating this influence, we compared $LSCF_{113}$ c_o values with LSC_{113} c_o values. However, calculated c_o values for $LSCF_{113}$ was only ~1 - 2 % different from those for LSC_{113}. We therefore decide to use c_o values for $LSCF_{113}$ for all samples.

VSC, indicative of changes in the oxygen nonstoichiometry induced by changes in the electrical potential, can be obtained from EIS data via the expression[14]

$$VSC = [1/(A_{electrode} \bullet \text{thickness})]((R_{ORR})^{1-n}Q)^{1/n}, \quad (3)$$

where Q is the non-ideal "capacitance", and n is the non-ideality factor of *CPE*. The fitted values of n for semi-circle CPE_{ORR} were found to range from ~ 0.96 to 1.0 over the entire pO_2 range examined (n =1, ideal).

Table S1. Constrained and relaxed lattice parameters of $LSCF_{113}$, $LSCF_{113}$ with the ~3 nm single-layer decoration of mixed LSC_{214} and LSC_{113} and the double-layer decoration of stacked ~3 nm LSC_{214} and ~0.5 nm LSC_{113} extracted from normal and off-normal XRD data at room temperature. Constrained normal and in-plane lattice parameters of all films were calculated from combining the inter-planar distance of the $LSCF_{113}$ $(002)_{pc}$ and $LSCF_{113}$ $(202)_{pc}$ peaks.

Samples	Constrained in-plane a / Å	Constrained normal c / Å	Relaxed lattice parameter $\hat{a}$ / Å	In-plane strain $\varepsilon_{aa} = \frac{(a-\hat{a})}{\hat{a}}$ / %	Normal strain $\varepsilon_{cc} = \frac{(c-\hat{a})}{\hat{a}}$ / %
LSCF ref.	3.897	3.899	3.898	-0.038	0.025
LSC_{214}	3.897	3.902	3.900	-0.077	0.051
$LSC82_{113}$:LSC_{214}	3.896	3.888	3.891	-0.013	0.088
$LSC64_{113}$:LSC_{214}	3.893	3.897	3.896	-0.068	0.045
$LSC46_{113}$:LSC_{214}	3.891	3.906	3.900	-0.023	0.015
$LSC82_{113}$ + LSC_{214}	3.905	3.903	3.903	-0.028	0.019
$LSC64_{113}$ + LSC_{214}	3.893	3.912	3.904	-0.029	0.019
$LSC46_{113}$ + LSC_{214}	3.899	3.907	3.904	-0.013	0.089

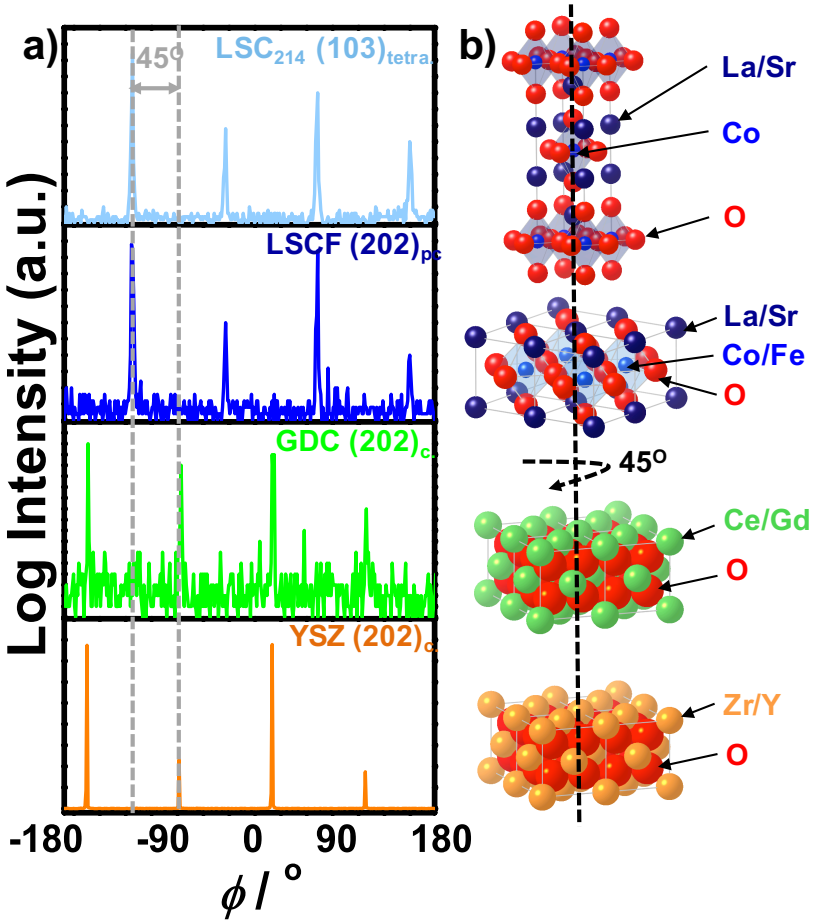

Figure S1. (a) off-normal XRD of a $LSCF_{113}$ sample with ~3 nm LSC_{214} coverage, and (b) schematic of the crystallographic rotational relationships among the $LSC_{214}(001)_{tetra.}$, $LSCF_{113}(001)_{pc}$, $GDC(001)_{cubic}$, and $YSZ(001)_{cubic}$.

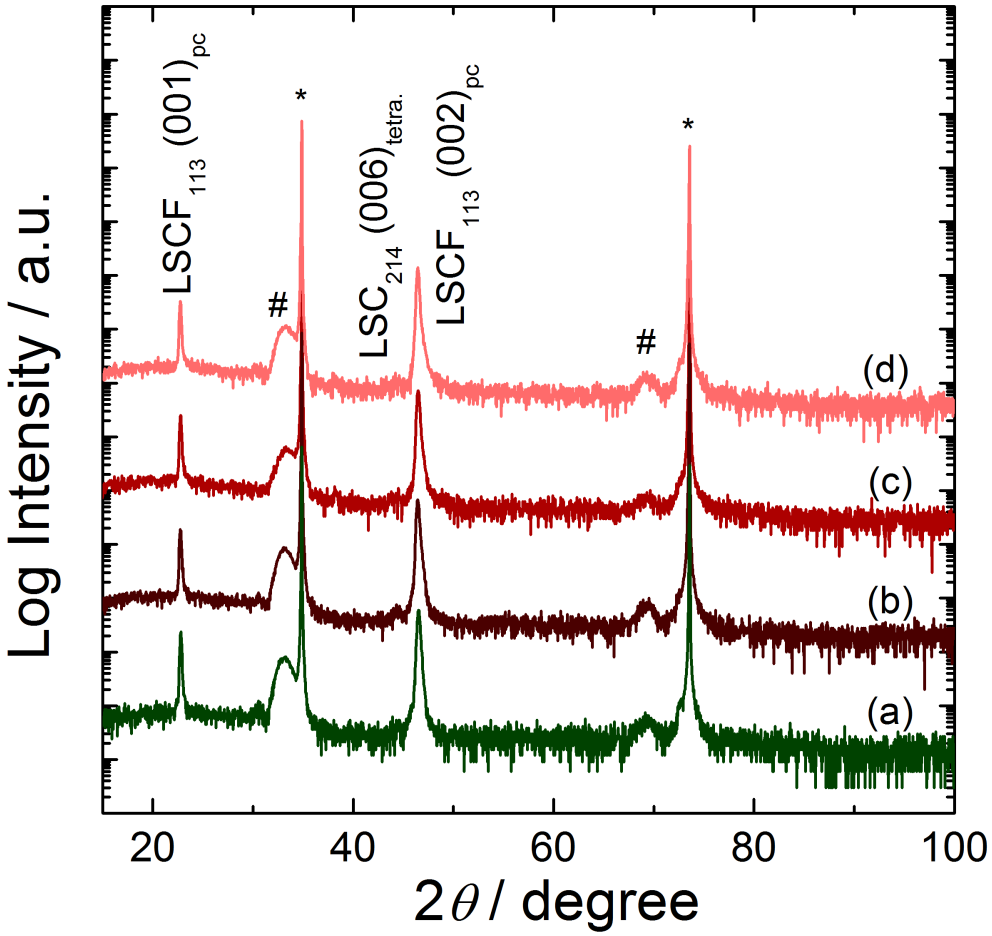

Figure S2. High-resolution X-ray diffraction analysis of (a) the $LSCF_{113}$ refernce (green), (b) the $LSCF_{113}$ with double-layer decorations of stacked $LSC46_{113}$ 25%:LSC_{214} 75% (dark red), (c) $LSC46_{113}$ 50%:LSC_{214} 50% (red), and $LSC46_{113}$ 75%:LSC_{214} 25% (light red) epitaxial thin flims on (001) YSZ substrates with GDC buffer layer. YSZ substrate and GDC peaks are indicated with pounds (#) and asterisks (∗), respectively.

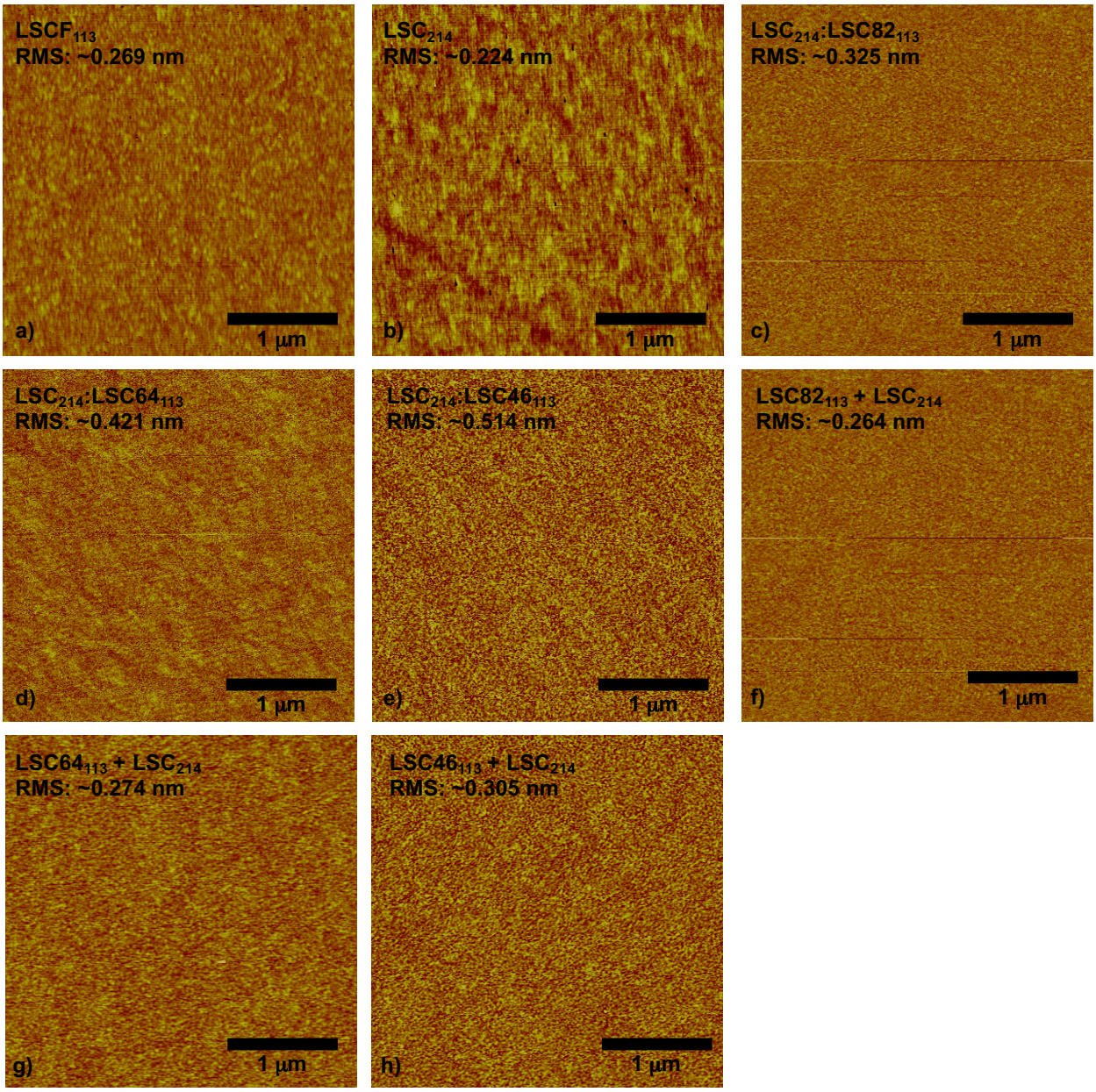

Figure S3. AFM images of (a) the ~65 nm $LSCF_{113}$ reference, (b) the ~3 nm LSC_{214}-decorated $LSCF_{113}$, and (c) the $LSCF_{113}$ with ~3 nm single layer decorations of mixed LSC_{214} and $LSC82_{113}$, (d) $LSC64_{113}$, and (e) $LSC46_{113}$ and the $LSCF_{113}$ with double-layer decorations of stacked ~3 nm LSC_{214} and (f) ~0.5 nm $LSC82_{113}$, (g) ~0.5 nm $LSC64_{113}$, and (h) ~0.5 nm $LSC46_{113}$ epitaxial thin films on (001) YSZ substrates with GDC buffer layer.

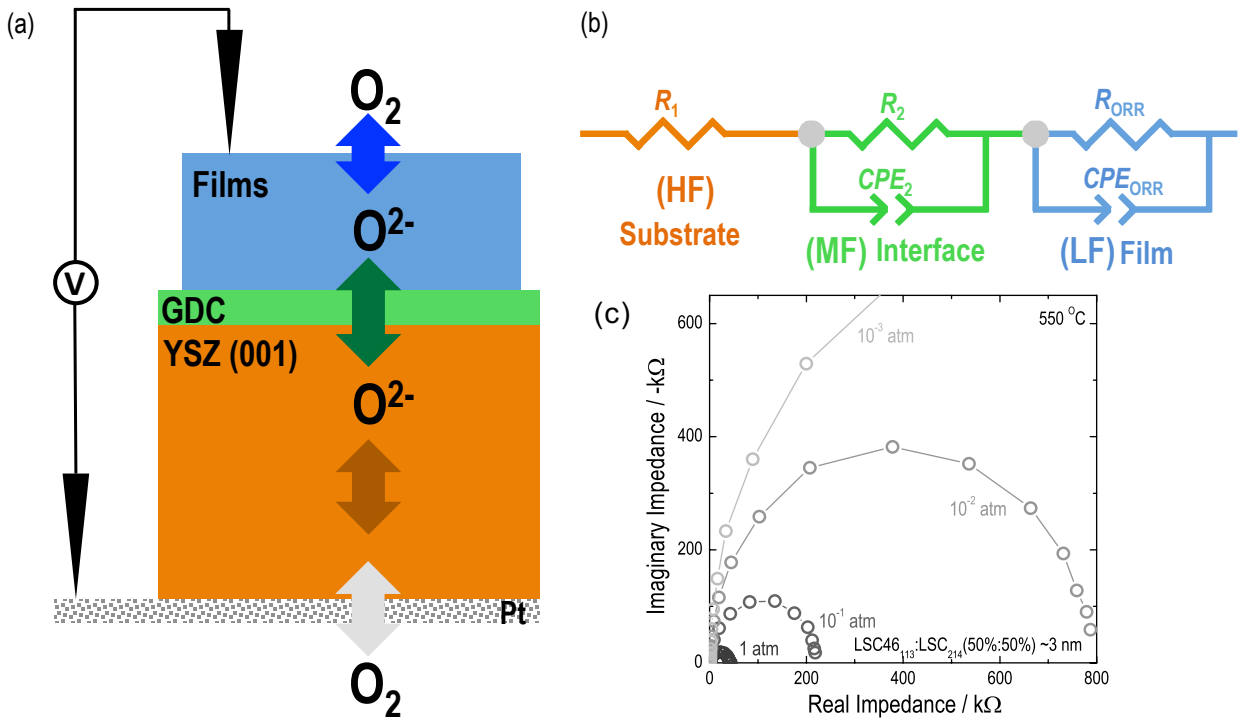

Figure S4. (a) Schematic of a LSCF/GDC/YSZ(001)/porous Pt samples and electrochemical testing configuration (not drawn to scale), and (b) equivalent circuit (R1 = YSZ electrolyte resistance, R2 = electrode/electrolyte interface resistance[4], R_{ORR} = ORR resistance, CPE = constant phase element) used to extract ORR kinetics, and (c) Nyquist plot of the $LSCF_{113}$ with a single layer decoration of LSC_{214} mixed with $LSC46_{113}$ thin films at 550 ºC;

References

1. M. Pechini: *U.S. Patent No. 3,330,697* (1967).
2. H.M. Christen, E.D. Specht, S.S. Silliman and K.S. Harshavardhan: Ferroelectric and antiferroelectric coupling in superlattices of paraelectric perovskites at room temperature. *Phys. Rev. B* **68**, 4 (2003).
3. E.J. Crumlin, E. Mutoro, Z. Liu, M.E. Grass, M.D. Biegalski, Y.L. Lee, D. Morgan, H.M. Christen, H. Bluhm and Y. Shao-Horn: Surface strontium enrichment on highly active perovskites for oxygen electrocatalysis in solid oxide fuel cells. *Energy Environ. Sci.* **5**, 6081 (2012).
4. G.J. la O, S.J. Ahn, E. Crumlin, Y. Orikasa, M.D. Biegalski, H.M. Christen and Y. Shao-Horn: Catalytic Activity Enhancement for Oxygen Reduction on Epitaxial Perovskite Thin Films for Solid-Oxide Fuel Cells. *Angew. Chem.-Int. Edit.* **49**, 5344 (2010).
5. S.B. Adler: Factors governing oxygen reduction in solid oxide fuel cell cathodes. *Chem. Rev.* **104**, 4791 (2004).
6. S.B. Adler, J.A. Lane and B.C.H. Steele: Electrode kinetics of porous mixed-conducting oxygen electrodes. *J. Electrochem. Soc.* **143**, 3554 (1996).
7. T. Kawada, J. Suzuki, M. Sase, A. Kaimai, K. Yashiro, Y. Nigara, J. Mizusaki, K. Kawamura and H. Yugami: Determination of oxygen vacancy concentration in a thin film of $La_{0.6}Sr_{0.4}CoO_{3-\delta}$ by an electrochemical method. *J. Electrochem. Soc.* **149**, E252 (2002).
8. Y.L. Yang, C.L. Chen, S.Y. Chen, C.W. Chu and A.J. Jacobson: Impedance studies of oxygen exchange on dense thin film electrodes of $La_{0.5}Sr_{0.5}CoO_{3-\delta}$. *J. Electrochem. Soc.* **147**, 4001 (2000).

9. P.S. Manning, J.D. Sirman, R.A. DeSouza and J.A. Kilner: The kinetics of oxygen transport in 9.5 mol % single crystal yttria stabilised zirconia. *Solid State Ion.* **100**, 1 (1997).

10. J. Maier: On the correlation of macroscopic and microscopic rate constants in solid state chemistry. *Solid State Ionics* **112**, 197 (1998).

11. J. Maier: Physical Chemistry of Ionic Materials: Ions and Electrons in Solids (John Wiley, Chichester, England ; Hoboken, NJ, 2004).

12. J. Fleig and J. Maier: The polarization of mixed conducting SOFC cathodes: Effects of surface reaction coefficient, ionic conductivity and geometry. *J. Eur. Ceram. Soc.* **24**, 1343 (2004).

13. J. Mizusaki, Y. Mima, S. Yamauchi, K. Fueki and H. Tagawa: Nonstoichiometry of the perovskite-type oxides $La_{1-x}Sr_xCoO_{3-\delta}$. *J. Solid State Chem.* **80**, 102 (1989).

14. J. Fleig: The grain boundary impedance of random microstructures: numerical simulations and implications for the analysis of experimental data. *Solid State Ion.* **150**, 181 (2002).